Int J Earth Sci (Geol Rundsch) (2016) 105:1681–1692
DOI 10.1007/s00531-014-1047-0

ORIGINAL PAPER

Seismic anisotropy of the lithosphere/asthenosphere system beneath the Rwenzori region of the Albertine Rift

B. Homuth · U. Löbl · A. G. Batte · K. Link · C. M. Kasereka · G. Rümpker

Received: 19 December 2013 / Accepted: 11 June 2014 / Published online: 2 July 2014

Abstract Shear-wave splitting measurements from local and teleseismic earthquakes are used to investigate the seismic anisotropy in the upper mantle beneath the Rwenzori region of the East African Rift system. At most stations, shear-wave splitting parameters obtained from individual earthquakes exhibit only minor variations with backazimuth. We therefore employ a joint inversion of SKS waveforms to derive hypothetical one-layer parameters. The corresponding fast polarizations are generally rift parallel and the average delay time is about 1 s. Shear phases from local events within the crust are characterized by an average delay time of 0.04 s. Delay times from local mantle earthquakes are in the range of 0.2 s. This observation suggests that the dominant source region for seismic anisotropy beneath the rift is located within the mantle. We use finite-frequency waveform modeling to test different models of anisotropy within the lithosphere/asthenosphere system of the rift. The results show that the rift-parallel fast polarizations are consistent with horizontal transverse isotropy (HTI anisotropy) caused by rift-parallel magmatic intrusions or lenses located within the lithospheric mantle—as it would be expected during the early stages of continental rifting. Furthermore, the short-scale spatial variations in the fast polarizations observed in the southern part of the study area can be explained by effects due to sedimentary basins of low isotropic velocity in combination with a shift in the orientation of anisotropic fabrics in the upper mantle. A uniform anisotropic layer in relation to large-scale asthenospheric mantle flow is less consistent with the observed splitting parameters.

Keywords East African Rift system · Albertine Rift · Seismic anisotropy · Shear-wave splitting · Joint splitting analysis · Waveform modeling

Electronic supplementary material The online version of this article (doi:10.1007/s00531-014-1047-0) contains supplementary material, which is available to authorized users.

B. Homuth (✉) · U. Löbl · G. Rümpker
Institute of Geosciences, Goethe University Frankfurt, Altenhöferallee 1, 60438 Frankfurt am Main, Germany
e-mail: homuth@geophysik.uni-frankfurt.de

A. G. Batte
Geology Department, Makerere University, Kampala, Uganda

K. Link
Institute for Geosciences, Johannes Gutenberg University Mainz, Mainz, Germany

K. Link
Gubelin Gem Lab Ltd., Luzern, Switzerland

C. M. Kasereka
Goma Volcano Observatory, Goma, North Kivu, Democratic Republic of Congo

Introduction

The East African Rift system (EARS) represents one of the world's largest continental rift structures (Bendick et al. 2006; Chorowicz 2005; Ebinger 1989). Starting at the Afar triple junction in the north, it extends approximately in N–S direction through East Africa. South of the Main Ethiopian Rift, the system splits up into two branches: the Albertine Rift in the west and the Kenya Rift in the east, enclosing the Tanzania Craton (Nyblade and Brazier 2002). The system continues as the Malawi Rift to the south and terminates at the coast of southern Mozambique. The Albertine Rift stretches 2,100 km from Lake Albert in the north to Lake Malawi in the south. It separates the Nubian

Plate to the west from the smaller Victoria plate to the east with a current extension rate of about 2 mm/a (Stamps et al. 2008). The Rwenzori region forms part of the Albertine Rift; it is located within approximately 0°N–1°N and 29.5°E–30.5°E and transected by the international border between Uganda and the Democratic Republic of Congo. The Rwenzori range is composed of Precambrian rocks and is situated within the rift valley reaching altitudes of about 5,100 m. The causes for the extreme uplift within an extensional setting are currently being investigated within the framework of the RiftLink research group. Results from recent geodynamic modeling suggest that the uplift of the Rwenzori range is caused by melt-induced alteration and delamination of mantle lithosphere between two neighboring rift segments (Wallner and Schmeling 2010). Volcanism and receiver functions indicate that the lithosphere beneath the Rwenzori region measures at least 120–140 km (Rosenthal et al. 2009; Wölbern et al. 2012). Potential explanations could either be that the thick lithosphere is a relictic cratonic (thick) root or the thickened lithosphere is the result of a paleoproterozoic crustal scaled north trending shear zone (Link et al. 2010).

The study of seismic anisotropy provides a unique link between mantle-deformation processes and observations of seismic waveform effects. The analysis of SKS splitting is a standard tool to infer the seismic anisotropy of the lithosphere/asthenosphere system. The spatial distribution of the two splitting parameters ϕ (polarization direction of the fast shear wave) and δt (delay time between fast and slow shear wave) is essential for the investigation of anisotropic structures and associated dynamic mantle processes and was investigated in numerous studies in the past (e.g., for reviews: Fouch and Rondenay 2006; Long and Silver 2009). The orientation of the anisotropic fabric can be derived from the polarization of the fast shear wave, while the extent and strength of the anisotropy is proportional to the delay time. Seismic anisotropy in the upper mantle is often thought to be controlled by the alignment of the *a*-axis of olivine through dislocation creep (Karato 2003; Ben Ismail and Mainprice 1998; Zhang and Karato 1995; Nicolas and Christensen 1987). Nevertheless, shape-preferred orientation due to magmatic dike intrusion in the lower lithosphere can have a significant influence on seismic anisotropy (Holtzman and Kendall 2010; Kendall et al. 2005; Gao et al. 2010). In case of continental rifting processes, several possible sources of seismic anisotropy must be considered. Vauchez et al. (2000) state that these sources are lithospheric deformation, asthenospheric flow and oriented melt pockets in the asthenospheric mantle. For the EARS, a transtensional lithospheric rupture model, as suggested by Nicolas et al. (1994) and Vauchez et al. (2000), leads to a restriction of the asthenospheric flow to the rift axis, generating a fast-polarization direction of the shear wave parallel to the rift. Additionally, an alignment of melt lenses in the asthenospheric wedge may account for a significant part of the seismic anisotropy (Vauchez et al. 2000).

The seismic anisotropy of the EARS has been investigated by previous studies, i.e., Walker et al. (2004) analyzed broadband data from stations in Tanzania, Kenya and Uganda. The obtained splitting parameters could be best explained by a lateral varying single-layer model of anisotropy with a horizontal fast axis. One essential insight of this study was that a lattice preferred orientation of olivine induced by extension could be excluded as the dominant factor for the anisotropy since the shear-wave splitting results showed no evidence of a ductile thinning of the lithospheric mantle by dislocation creep. Walker et al. (2004) indicated that the extension in East Africa occurs by magmatic intrusions in narrow rift zones possibly supported by a fossilized anisotropy in the lithosphere due to past orogenic events. Kendall et al. (2005) analyzed shear-wave splitting in the Afar region in Ethiopia. They observed a fast-polarization direction parallel to the strike of the rift with delay times in the range between 1 and 3 s. Correlating the anisotropic structures and the orientation of dikes in the magmatic segments of the Afar region, Kendall et al. (2005) suggest that the anisotropy is a result of melt-filled cracks accompanied by a low spreading of the crust, supporting a magmatic rifting model with an initially thick continental lithosphere. Vertical magmatic dikes in the lithosphere were also proposed by Gao et al. (1997) to explain parallel fast-polarization directions observed in the Baikal Rift and the Kenya Rift. Gao et al. (2010) reanalyzed data recorded in the Afar Depression, the Main Ethiopian Rift and the Ethiopian Plateau finding rift-parallel fast directions that can be explained by a single layer of anisotropy for the Ethiopian Plateau and the Main Ethiopian Rift. Nevertheless, data from the Afar Depression showed a systematic azimuthal dependence of splitting parameters with a $\pi/2$ periodicity suggesting a two-layer model of anisotropy. Gao et al. (2010) explained the fast directions in the top layer by magmatic dikes in the lithosphere, while the fast directions and delay times in the second layer could best be explained by anisotropy due to a flow in the asthenosphere beneath the Main Ethiopian Rift and the Afar Depression. Hammond et al. (2010) investigated the ability of shear-wave splitting to constrain spatial variations in anisotropy using a one-way wave equation modeling scheme. They showed that lateral variations in anisotropy on the order of 20–50 km can be identified by shear-wave splitting and they used their modeling results to interpret the shear-wave splitting measurements in the Main Ethiopian Rift by Kendall et al. (2005). To explain the measured splitting parameters, Hammond et al. (2010) modeled a 100-km-wide rift zone with 7–9 % anisotropy and a depth of the anisotropy

starting at 90 km, which is the supposed depth of melt initiation beneath the Main Ethiopian Rift. Bagley and Nyblade (2013) examined shear-wave splitting measurements of SKS and SKKS phases in eastern Africa, revealing an overall pattern of NE-aligned polarization directions being consistent with mantle flow from the African superplume. They also indicate a connection between lower mantle processes and near surface tectonic deformation. Besides this overall pattern associated with the African superplume, they acknowledge the possibility of anisotropy due to magma-filled cracks in the lithosphere within the rift regions.

In this paper, we present results from a temporary seismic network located around the Rwenzori region of the Albertine Rift. The study aims to constrain anisotropy and mantle-deformation processes in relation to the formation of the rift zone. Local and teleseismic earthquake recordings are used to image structures of the crust and upper mantle within the region. We provide detailed estimates of the magnitude and orientation of anisotropic structures in the Rwenzori region obtained from shear-wave splitting analyses and numerical waveform modeling. These results will improve the general insight into the mechanisms of active rifting and are essential for a better understanding of the rifting processes in the western branch of the EARS.

RiftLink seismic networks and data set

The RiftLink project was conducted over a time period of about 6 years from 2006 to 2012. The project was divided into two phases. During phase I, a temporary network consisting of 32 mobile broadband and short-period seismic stations, covering an area of approximately 140 × 90 km^2, was operating from February 2006 to December 2007 (Fig. 1). A detailed description of the station setup of phase I can be found in Lindenfeld et al. (2012). Phase II of the RiftLink project was conducted between September 2009 and March 2012 consisting of 32 seismic broadband stations spread out around the Rwenzori Mountains, both on the Ugandan and the neighboring Congolese side (Fig. 1). In contrast to phase I, the stations were more evenly distributed throughout the region, covering an area of about 220 × 170 km^2. Trillium 120P, Trillium Compact and Guralp CMG-3T sensors in combination with Taurus and EDL data loggers recorded continuously at a sample rate of 100 Hz. Additionally, for the shear-wave splitting analysis, data from the permanent station MBAR (part of the Global Seismographic Network GSN) were analyzed.

Only earthquakes with magnitudes exceeding a value of $M_w = 6.0$ and an epicentral distance of at least 85° were considered in the shear-wave splitting analysis. For epicentral distances less than 85°, contamination from other shear-wave phases in the seismograms is likely (Long and

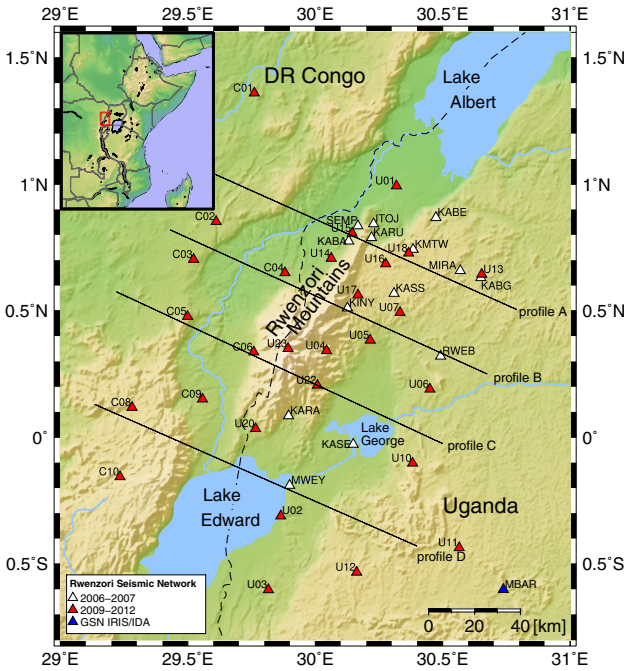

Fig. 1 Seismic station networks in the Rwenzori region. *White triangles* represent stations of the first phase of the RiftLink project from February 2006 to December 2007; *red triangles* mark stations of the second phase from September 2009 to March 2012; and the GSN station Mbarara is marked by a *blue triangle*. Splitting measurements along four profiles (*lines* across the rift) are shown in Fig. 6

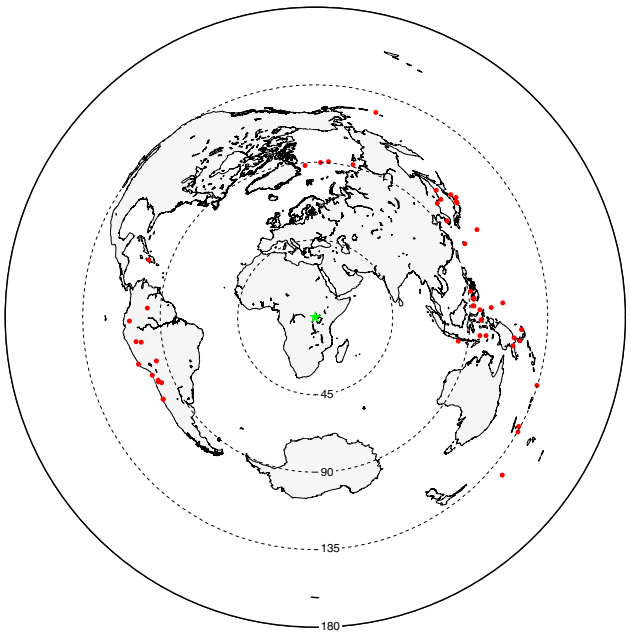

Fig. 2 Distribution of earthquakes used in this study. The *circles* indicate epicentral distances of 45°, 90°, 135° and 180°. The *red dots* mark epicenters of earthquakes contributing to the SKS splitting analyses. The *green asterisk* in the center of the map corresponds to the location of our networks

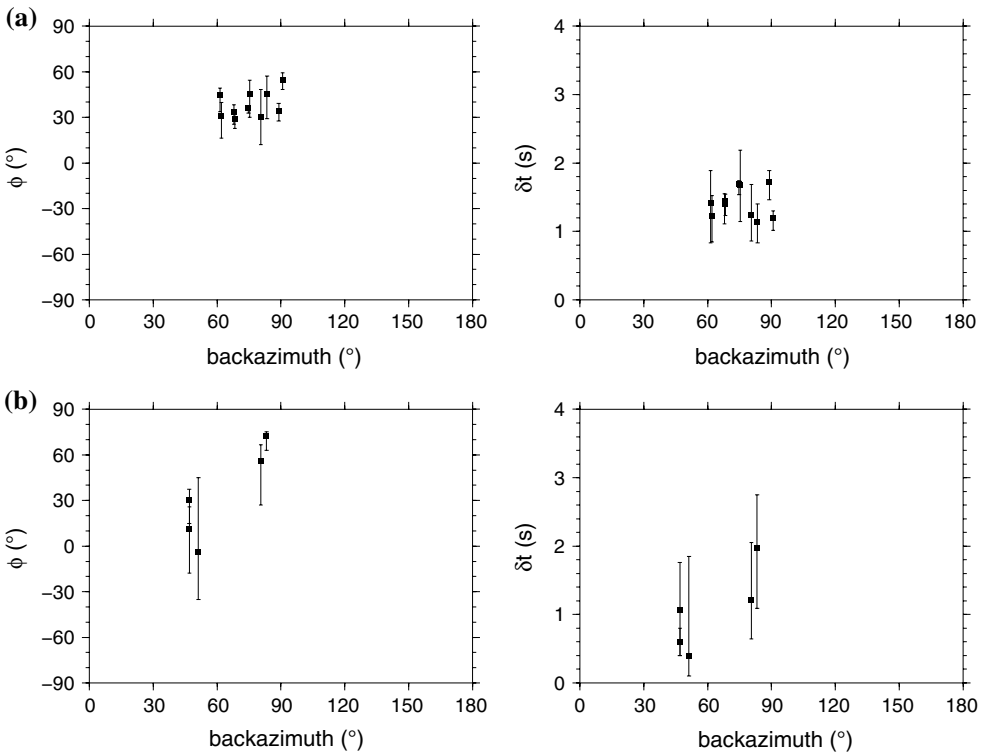

Fig. 3 Splitting parameters shown as a function of the backazimuth. **a** Fast axis and delay time including 95 % confidence level for station C02 for which a joint splitting analysis was conducted. **b** Fast axis and delay time including 95 % confidence level for station U18 showing an azimuthal dependence of the splitting parameters with backazimuth, and thus, no joint splitting analysis was conducted for this station

Silver 2009). We also restricted our analysis to events that showed a clear SKS phase onset on the radial component with a good signal-to-noise ratio. This restriction led to a total number of 50 earthquakes that produced at least one well-defined measurement. The majority of the earthquakes are from the western Pacific and South American subduction zones (Fig. 2, supplementary Table S1). A further reduction in the cutoff magnitude did not lead to any useful additional measurements, mainly because the SKS phase onsets could not be distinguished from the background noise at lower magnitudes. In total, 43 stations produced at least one well-defined SKS splitting measurement.

Data analysis and results

Splitting parameters from SKS phases

The 50 teleseismic earthquakes used for the analysis produced 160 SKS splitting measurements. The splitting parameters were determined by minimization of the transverse SKS component, as described by Silver and Chan (1991). For most of the stations, an investigation of variations in splitting parameters as a function of the backazimuth showed no visible trends (Fig. 3a, shows an example of station C02), yet for many stations, there is only limited azimuthal coverage (supplementary Fig. S1). However, eight stations (two on the Congolese side and six on the eastern rift shoulder) showed evidence of a possible azimuthal dependence of the splitting parameters (Fig. 3b, shows an example of station U18). Insignificant azimuthal variations in the splitting parameters imply a single layer of anisotropy (or multiple layers with similar or orthogonal fast directions) and therefore allow the application of a joint splitting analysis. In case of azimuthal dependences of the splitting parameters, which could be a result of, i.e., a plunging symmetry axis or vertical changes of anisotropic properties (Savage 1999; Rümpker and Silver 1998), it is not possible to apply this joint splitting analysis. For the joint splitting analysis, we determined splitting parameters that best minimize the sum of the transverse energy of all recorded earthquakes at one station, similar to the method introduced by Wolfe and Silver (1998). This approach leads to a single pair of splitting parameters that characterizes the anisotropic properties beneath a station. For both, the joint and the single event analysis, the original seismograms were band-pass filtered in the 0.02–0.25 Hz range and then rotated in the radial–transversal coordinate system. The SKS time window for the analysis is visually identified and adjusted if necessary to exclude other phase onsets. Corrections to the theoretical backazimuth are applied in cases where the sensors are misoriented. Fifty random time windows around the chosen SKS phase are selected to identify the particular time window that best minimizes the total transverse energy. Splitting parameters are calculated for all of these 50 random time windows to estimate the

influence of noise on the measurements. This influence can be quantified by calculating the mean splitting parameters and their standard deviations based on the results of all 50 random trials. For the final analysis, the optimum time window is chosen automatically based on the minimization results of all 50 time windows. The uncertainties in the measurements are calculated using this time window based on a 95 % confidence level.

An example of a joint splitting analysis for station C03 is shown in Fig. 4a, b shows the original radial and transverse components of two earthquakes contributing to the joint splitting analysis. Also shown are the corrected waveforms after applying an inverse splitting operator, which is defined by the splitting parameters from the joint splitting analysis. The contour plot of the energy of the transverse component (Fig. 4c) includes the range of splitting parameters with 95 % confidence level. Figure 4d, e shows the original particle motions in a radial/transversal coordinate system as well as the corrected particle motions. The application of the inverse splitting operator leads to a linearization of the particle motion for both earthquakes.

For most of the stations, two to five individual SKS measurements contributed to the joint analysis while 13 stations only showed one well-defined SKS onset. However, for some stations, up to 16 SKS measurements were obtained. The results of the joint splitting analysis in combination with the results of the single analysis for the stations showing azimuthal dependence on the splitting parameters are presented in Fig. 5 and in supplementary Table S2. The mean splitting delay time is 1.03 ± 0.39 s, which is roughly the global average of 1.0 s for continental areas (Silver 1996). Larger delay times are observed within the center of the rift to the north and to the south of the Rwenzori with values of δt reaching up to 1.9 s. Smaller delay times are found along the graben shoulders, with a stronger decrease to the east. Here, δt decreases to around 0.4–0.7 s. The dominant pattern of fast directions is aligned parallel to the strike of the rift system in NE–SW direction. A deviation from this trend can only be observed in the southern rift segment in the area between Lake Edward and Lake George. Here, the fast polarizations shift to a more N–S orientation. This deviation in the fast polarizations diminishes with greater distance to the rift leading to a NE–SW orientation in the southeastern part of the study area. Figure 6 shows variations in splitting parameters along the profiles outlined in Fig. 1. Profiles A to C show largely scattered results, mainly because at some stations, joint splitting analysis was not applied due to azimuthal variations in the splitting parameters. Profile D is the only profile for which all results are based on a joint splitting analysis. The splitting parameters exhibit relatively systematic variations. Here, we attempt to investigate and explain the systematic and relatively pronounced changes over a short scale (in the center of profile D) by a comparison with results from waveform modeling in "Waveform modeling of short-scale splitting variations" section.

Splitting parameters from local earthquakes

To better constrain the depth origin of the anisotropic regions, we conducted a splitting analysis of S phases from a total of over 7,000 local earthquakes. A detailed analysis of the crustal splitting results is described in Batte et al. (2014). At most stations, the delay time δt is much smaller (0.01–0.1 s, Fig. 7) than the worldwide average for crustal shear-wave splitting (0.1–0.3 s) as specified by Silver (1996). On average, the delay time δt associated with crustal sources beneath the Rwenzori region is ~0.04 s. For some stations, there was no evidence of shear-wave splitting. Additionally, a sequence of seven local earthquakes with focal depths between 50 and 60 km was used to derive splitting parameters. These deep earthquakes originate from the upper lithosphere and are likely caused by magmatic impregnation of the mantle lithosphere (Lindenfeld and Rümpker 2011). The average delay time obtained from these deep local earthquakes is $\delta t = 0.18$ s and thus larger than the one observed in the crust, but still not even close to delay times obtained from teleseismic earthquakes (~1 s), indicating that crustal anisotropy is negligible and thus suggesting that the dominant source region for seismic anisotropy beneath the rift is located within the mantle.

Discussion

Compared with splitting measurements in other parts of the EARS (Gao et al. 2010; Kendall et al. 2005), the splitting parameters in the Rwenzori region exhibit smaller delay times but a similar pattern of fast-polarization directions. For two stations located within the area of interest of this paper (one station near Lake Edward and the other at the northern end of the Rwenzori Mountains), Bagley and Nyblade (2013) derived similar splitting parameters, both in the orientation of the fast axes and the delay times.

The causes of anisotropy in the Rwenzori region have to be located in the upper mantle, since the analysis of crustal S phases shows weak anisotropy that contributes less than 10 % to the delay times inferred from SKS measurements. Anisotropy in the upper mantle leading to SKS splitting may be attributed to either a lattice preferred orientation (LPO) of anisotropic minerals such as, e.g., olivine (Nicolas and Christensen 1987) or a shape-preferred orientation (SPO) formed by, e.g., vertically aligned magmatic dikes. To explain the observed anisotropy pattern, we discuss a range of possible models.

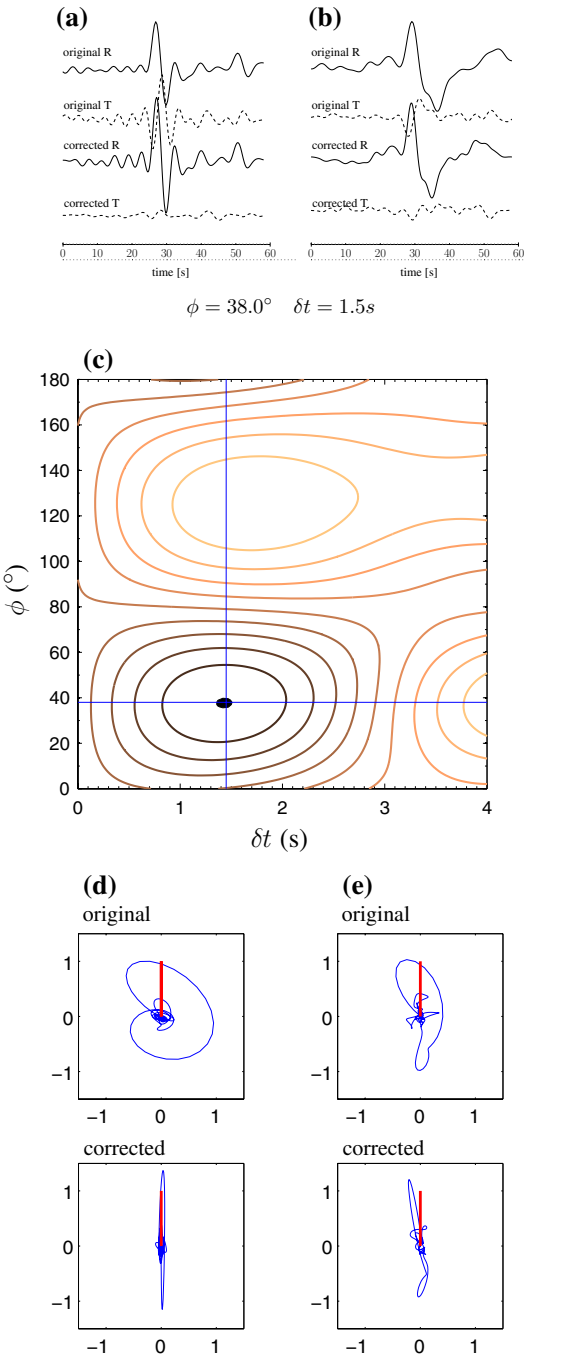

Fig. 4 Example of a joint splitting analysis for station C03, showing two earthquakes that contributed to the inversion. **a**, **b** Original and corrected radial and transverse SKS arrivals for two earthquakes simultaneously analyzed in the joint splitting analysis. **c** Contour map of the normalized energy sum of the corrected transverse components plotted as a function of the splitting parameter ϕ and δt. The *blue cross marks* the pair of splitting parameters that best minimizes the total energy on the transverse components for both earthquakes. The 95 % confidence level is shown as the blackened area. **d** Particle motion patterns of the normalized original and corrected radial and transverse components shown in **a**. **e** Same as in **d** but for the components shown in **b**. Splitting parameters given on top of **c** were used for the linearization of the particle motions. The *red line* in **d**, **e** represents the theoretical backazimuth

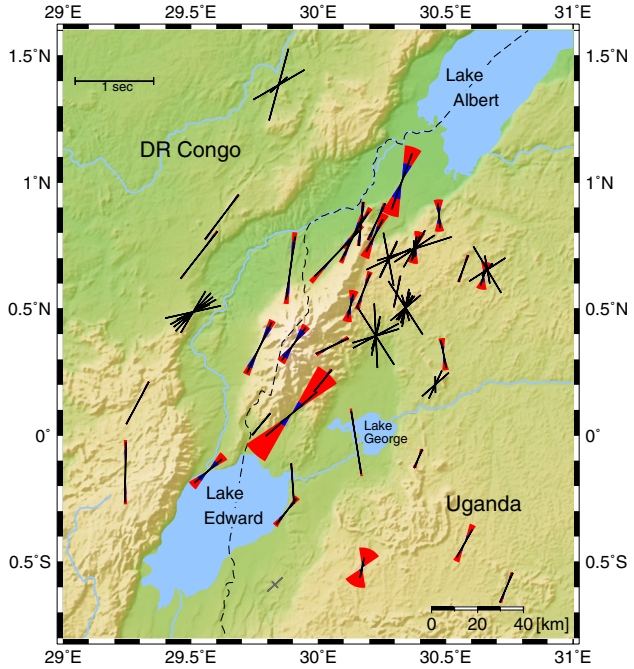

Fig. 5 SKS splitting parameters from the joint and single splitting analysis. The length of the *bars* corresponds to the delay time, and the angle to the north direction is identical to the fast direction. Ninety-five percent confidence levels for the joint splitting and the single measurements are marked by *blue* and *red* sectors. Ninety-five percent confidence levels for stations showing azimuthal dependence of the splitting parameters are given in Table S2. The *cross* in the *lower middle* represents a null measurement with possible fast or slow polarization axis along or orthogonal to the backazimuth of the earthquake

Asthenospheric-flow model

The asthenospheric drag beneath a lithospheric plate results in an alignment of olivine *a*-axes as a result of dislocation creep deformation associated with simple shear at the base of the plate (e.g., Tommasi 1998), assuming a flat geometry of the lithosphere/asthenosphere boundary. According to Wolfe and Silver (1998), the ϕ directions would be the absolute plate motion (APM) and the magnitude of δt would be rather constant over large geological domains (Heintz and Kennett 2005). The Victoria Plate on the eastern side of the rift system is moving in an ESE direction relative to the Nubian Plate on the western side (Stamps et al. 2008), and thus, for the Rwenzori region, this model can be ruled out because the observed ϕ directions (mainly NE–SW) show no consistency with the APM direction.

Cenozoic Rift-extension model

Investigations of seismic anisotropy in the Baikal Rift (Gao et al. 1994) showed ϕ directions parallel to the extension direction, which is consistent with an alignment of

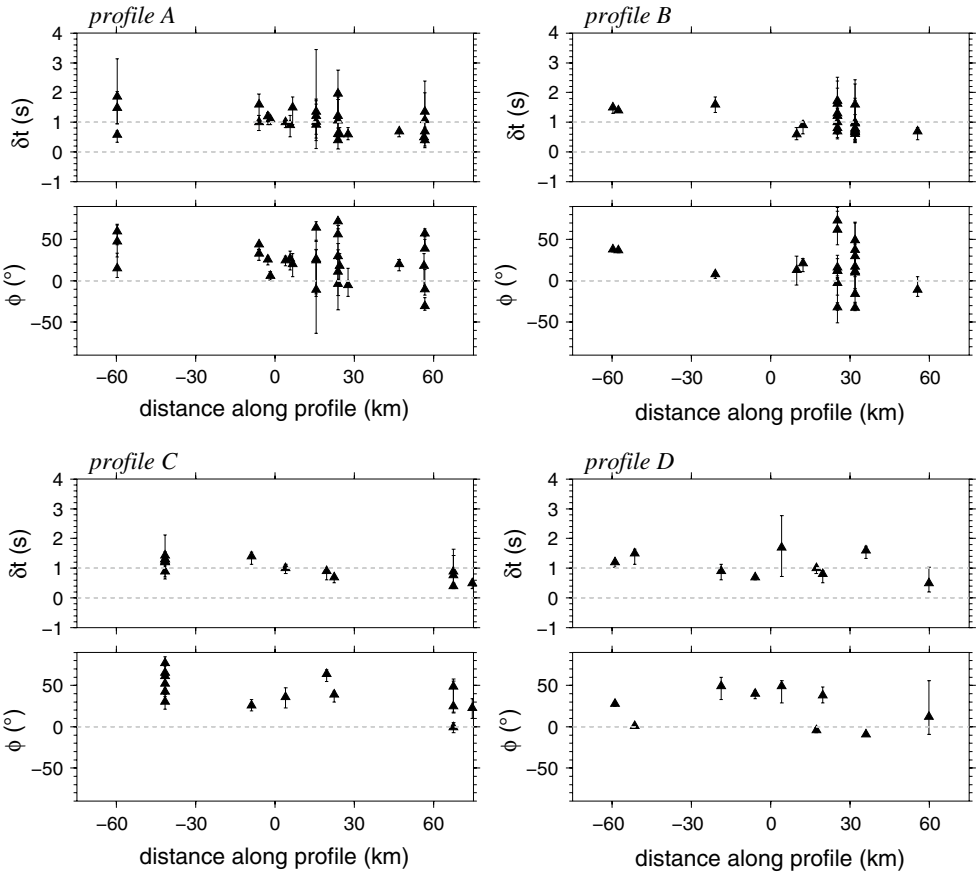

Fig. 6 SKS splitting parameters along *four profiles* across the rift as shown in Fig. 1. Each profile has a length of 150 km including all splitting measurements up to a distance of 30 km from the profile

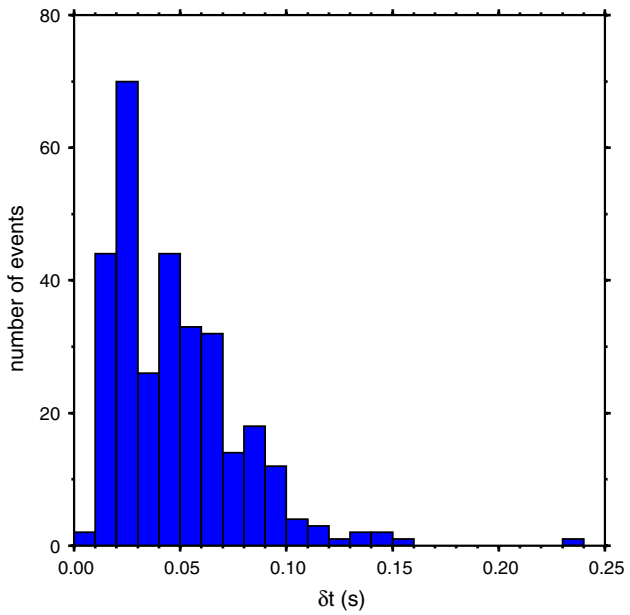

Fig. 7 Splitting parameters obtained from local earthquakes in the crust, showing an average delay time of $\delta t = 0.04$ s

olivine *a*-axes in this direction (Vauchez et al. 2000). For the Rwenzori region, a NW–SE to WNW–ESE direction of extension has been proposed by previous studies (Walker et al. 2004; Bosworth et al. 1992; Ebinger 1989; Sander and Rosendhal 1989). This is in agreement with T-axes orientations inferred from fault-plane solutions by Lindenfeld et al. (2012). However, the measured ϕ directions do not align with the proposed direction of Cenozoic Rift extension and thus implies that the anisotropic structures are not a result of the late-phase or present-day ESE extension. An extension-driven rift-perpendicular flow of mantle material is therefore ruled out as a plausible cause for the observed splitting parameters.

Plume upwelling/channel flow model

The rift-parallel orientation of anisotropy could be caused by a channeled horizontal flow of mantle material along the rift (Vauchez et al. 2000), possibly originating from the Afar plume in the northern EARS. However, this model seems unlikely, as there is no direct connection between the western branch and the northern section of the EARS. In fact, the western branch is restricted to the north by the Asawa-fault. A single mantle plume in the Afar region as proposed by Walker et al. (2004) can therefore not explain the dominant mechanism triggering the observed anisotropy in the Rwenzori region. Bagley and Nyblade (2013) state that only a mantle flow generated by the African superplume

is consistent with the observed fast-polarization directions in the Afro-Arabian Rift system away from volcanic rift valleys. However, large-scale mantle flow induced by the superplume cannot explain the small-scale variations in splitting parameters observed in the Rwenzori region (see "Waveform modeling of short-scale splitting variations" section below). Additionally, the characteristics of the low volume and highly potassic lavas exposed in the region do not support a plume upwelling model. The petrology rather points to low-degree melting of thick and altered lithosphere as the magmatic source for the West-Ugandan volcanic fields (Rosenthal et al. 2009; Foley et al. 2012). Plume upwelling normally is seen together with high-volume lavas such as in regions of the Kenya Rift.

Anisotropy due to alignment of parallel dikes or SPO of melt-filled lenses

Gao et al. (1997) discuss the alignment of melt-filled pockets as a possible cause for ϕ directions parallel to the trend of the rift. In this model, the long and short axes of the pockets are parallel and perpendicular to the main stress directions σ_1 and σ_3, respectively. The shape-preferred orientation (SPO) of water-filled or magma-filled lenses as cause for anisotropy has also been discussed by Crampin (1991), Kendall (1994). According to Walker et al. (2004), melt-filled dikes or lenses tend to align perpendicular to the minimum main stress direction σ_3. In the Rwenzori region, a WNW orientation of σ_3 is observed (Lindenfeld et al. 2012), which is almost perpendicular to the trend of the rift and also is consistent with rift-parallel fast-polarization directions. Furthermore, in such a case, delay times are expected to exhibit the largest values in the center of the rift. Delay times are thought to decrease with increasing distance from the rift due to the gradual freezing of the dikes/lenses. In the case of the Rwenzori region, we also find the largest delay times in the center of the rift (especially in the northern part of the study area; see profile A in Fig. 6). Wölbern et al. (2012) have also discussed the possibility of melt infiltration into the lithosphere. They located the upper boundary of this zone (the melt infiltration front, MIF) at a depth of about 60 km beneath the Rwenzori-section of the rift. The highly potassic and silica under-saturated lavas exposed in the region are consistent with small-scale veins within the lowermost lithosphere (Foley 1992) and thus also point to the possible existence of small-scale dikes and melt-filled lenses below the crust at a depth between 60 and 140 km (Rosenthal et al. 2009; Foley et al. 2012).

Waveform modeling of short-scale splitting variations

In the southern rift segment, especially in the area between Lake Edward and Lake George, a shift in fast directions from NW–SE to a more N–S direction can be observed (profile D in Fig. 6). This deviation in the fast directions diminishes with greater distance to the rift again leading to a NE–SW orientation in the southeastern part of the study area. These small-scale spatial variations cannot be explained by any of the models discussed above. It is also unlikely that the observed small-scale variations result from the uncertainties of the SKS measurements, which occur due to the noise on the analyzed window, since we evaluate this influence on the splitting results by calculating the splitting parameters for all of the 50 random time windows used in the splitting analysis. Uncertainties from the analysis of these 50 random time windows around the SKS phase, which characterize the noise influence, are in the range of only 1°–2° for the fast-polarization directions at almost all stations and can therefore not explain the observed small-scale variations. Based on Fresnel zone estimates (Rümpker and Ryberg 2000), these variations are likely attributed to causes of shallow origin (within the crust). Our study has shown that the anisotropy within the crust is rather insignificant ("Splitting parameters from local earthquakes" section). We therefore assume an influence of isotropic velocity variations in relation to sedimentary basins in combination with a change in the orientation of the dike intrusions in the upper mantle as possible causes.

To verify this, we test different models of isotropic/anisotropic velocity variations using two-dimensional finite-difference waveform modeling (see "Appendix" for further details, Fig. 8). We consider a vertical section (below profile D of Fig. 6) with a horizontal extension of 150 km and a depth extension of 250 km. In view of results obtained by Wölbern et al. (2012) and Gummert et al. (2014), the crustal thickness is set to 30 km, the upper boundary of the infiltrated lithosphere (MIF) to 60 km and the lithosphere–asthenosphere boundary (LAB) to 120 km. The crust is assumed to be isotropic. Between the MIF and the LAB, we assume melt infiltration by dike intrusions. We assume that this region can be modeled as an effective anisotropic medium characterized by transverse isotropy with a horizontal symmetry axis (HTI-medium). The anisotropic coefficients are derived using the theory of Backus (1962) applied to a medium with two alternating layers of different isotropic velocities. To obtain the observed overall pattern in ϕ, we separate this zone into two blocks with differently oriented symmetry axes (pointing to N0°W in the eastern block and N25°E in the western block). The plane wave traversing through the model is initialized in an isotropic region at the bottom with a period of 8 s and an initial polarization of 70°. In order to suppress the effects of artificial reflections from the boundaries, the computational grid is much larger than the immediate region of interest. Free surface conditions are specified at the upper

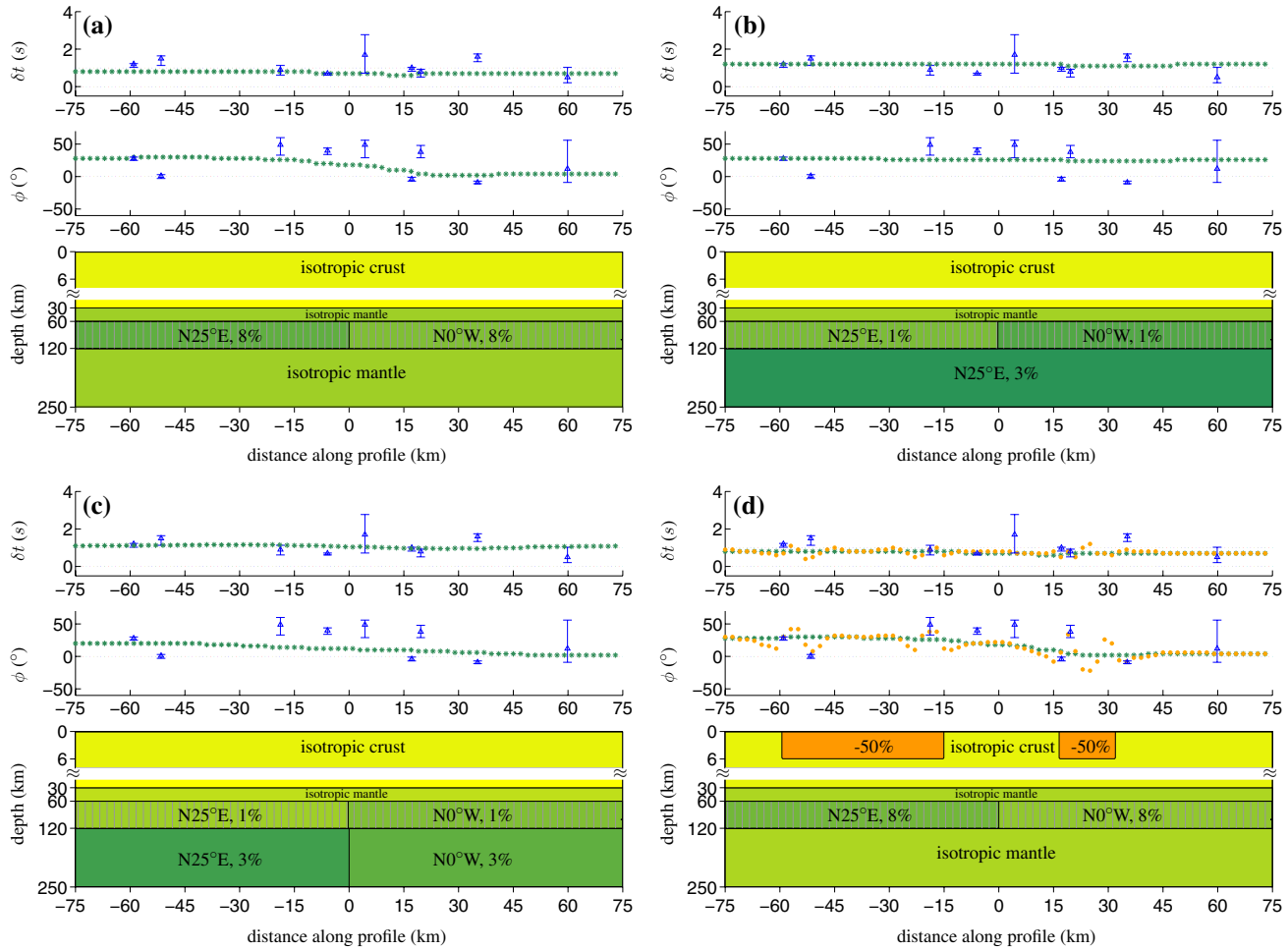

Fig. 8 Waveform modeling of splitting parameters along profile D shown in Figs. 1 and 6. The dike-induced seismic anisotropy is assumed to be located below 60 km and corresponds to layers of 8 % (**a**, **d**) and 1 % (**b**, **c**) of effective anisotropy, respectively. Two isotropic blocks with a velocity reduction of 50 % are inserted in **d** to simulate effects of sedimentary deposits. The *green stars* represent seismic parameters without sediment layers; the *orange dots* show variations in splitting parameters due to the sediment layers. The *blue triangles* show the measured splitting parameters along profile D

boundary of the computational grid. To determine the splitting parameters, synthetic seismograms are calculated at a distance interval of 2 km and are analyzed using the same procedure as in the case of real SKS waveforms. A similar modeling approach was used by Wölbern et al. (2014) for the interpretation of shear-wave splitting in the Andes. The upper panels in Fig. 8 show splitting parameters obtained from observed and synthetic waveforms. The green stars represent the splitting parameters for a model with a homogenous isotropic crust. The blue triangles show the observed splitting parameters along profile D. The region of effective anisotropy due to the aligned dikes is indicated by the hatched area. To fit the observed splitting parameters, an effective anisotropy of 8 % in the HTI-medium is needed. This effective anisotropy can be explained by a velocity difference of 33 % between the two layers of the HTI-medium. Nevertheless, this model of two anisotropic blocks is not able to explain the observed short-scale variations in the fast directions. In Fig. 8b, we consider an alternative model with a layer of rift-parallel olivine *a*-axes beneath the LAB. This model is to simulate mantle flow induced by the African superplume, as previously proposed by Bagley and Nyblade (2013). We assume 3 % of anisotropy within the asthenosphere down to a depth of 250 km. The elastic coefficients are taken from Kumazawa and Anderson (1969) and are scaled appropriately. To fit the observations in this case, the effective anisotropy of the HTI-medium is reduced to only 1 %. The results show that the sublithospheric flow has a dominant effect on the fast polarizations, such that lateral variations in splitting parameters cannot be accounted for. To fit the general pattern of the observed fast polarizations, the two blocks with different symmetry axes would have to continue further down (Fig. 8c). However, such a change in

the orientation of the olivine a-axis at relatively great depth seems unlikely. We, therefore, add two crustal low velocity zones (LVZ) to account for the effects of 6-km-thick sedimentary deposits (Fig. 8d). The velocity reduction in the LVZ is 50 %. Each LVZ has a significant influence on ϕ and δt (orange dots in Fig. 8d). Changes in ϕ of up to 34° and of 0.5 s in δt are achieved along the profile over distances of only 2 km. Also, the width of the LVZ has a great influence on the splitting parameters. The smaller LVZ on the eastern side of the rift has a stronger influence on the variation in the splitting parameters on a short scale. Only with extreme conditions, such as a strong velocity reduction (50 %) and a thickness of 6 km of the LVZ, can this simple model describe the observed variations in ϕ and δt. Results for an additional model that also includes mantle flow generated by the African superplume according to Bagley and Nyblade (2013) together with the crustal LVZs are shown in supplementary Fig. S2. However, in this case, small-scale variations in splitting parameters are (again) reduced.

Conclusions

To investigate the seismic anisotropy in the upper mantle beneath the Rwenzori region of the EARS, shear-wave splitting from local and teleseismic earthquakes has been analyzed. The fast polarizations obtained from 50 teleseismic events are generally rift parallel with an average delay time of about 1 s. Shear waves from local events within the crust show highly heterogeneous fast polarizations and average delay times of only $\delta t = 0.04$ s. Fast polarizations from local mantle earthquakes at depths of about 55 km exhibit intermediate delay times of 0.2 s. The observations suggest that the anisotropy in the Rwenzori region observed from teleseismic phases is located within the mantle lithosphere below about 60 km. Our results are consistent with rift-parallel magmatic intrusions within the lithosphere as it would be expected during the early stages of continental rifting. Synthetic modeling of shear-wave splitting for the southern part of the study area, where a shift in the orientation of the fast polarization axis has been detected, shows that the shift can partly be explained by a change in the orientation of the effective symmetry axes in the upper mantle from N0°W in the east to N25°E in the west. We are able to fit the observed short-scale variations in the splitting parameters by adding two LVZ in the upper crust (sedimentary basins in the rift). The effective anisotropic layer is most likely situated in a depth between 60 and 120 km, which is the depth range of melt infiltration propagating upwards from the LAB as proposed by Wölbern et al. (2012) for the Rwenzori region. Our modeling further indicates that the anisotropy is likely limited to the (lower) lithosphere, because anisotropy at greater depth caused by, e.g., a rift-parallel flow in the asthenosphere, smoothes the effects of the crustal LVZs on variations in ϕ and δt. We further note that 3-D isotropic and anisotropic velocity structures can have additional influences on the short-scale variations in the splitting parameters. However, waveform modeling of 3-D anisotropic structures and their influence on SKS splitting measurements will be part of future studies.

Acknowledgments Funding for this study was provided by the Deutsche Forschungsgemeinschaft (DFG). We thank the Geophysical Instrumentation Pool Potsdam (GIPP) for providing the seismological equipment and GEOFON for archiving the data. The support of the Ugandan National Council for Science and Technology and of the Ugandan Wildlife Authority is greatly appreciated. Data from station MBAR has been provided by GSN-IRIS/IDA. The manuscript significantly benefited from the constructive comments and suggestions of Tuna Eken and one anonymous reviewer.

Appendix

The numerical simulations of seismic wave fields presented in this paper are based on the heterogeneous wave equation

$$\rho \partial_t^2 u_i = \partial_{x_j} \left(C_{ijkl} \delta_{x_l} u_k \right),$$

where $i, j, k, l = 1, \ldots, 3$, ρ denotes the density, u_i is the displacement and C_{ijkl} is the elastic tensor. Changes in material properties are restricted to the vertical x_1, x_3 coordinate plane in a reduced 2-D Cartesian geometry. This implies that any spatial derivative δ_{x_2} vanishes. To discretize the wave equation on a grid, the finite-difference method is used up to the second-order approximation. The procedure is identical to Ryberg et al. (2002). An equidistant grid spacing of $\Delta x = \Delta z = 0.25$ km is assumed. A sampling rate of $\Delta t = 0.0175$ s was found to be suitable to insure a robust discretization. For the comparison with SKS phases, a period of $T = 8$ s is used. As side effects are to be neglected, the grid size is chosen much larger than the evaluated model area.

In this work, anisotropy due to shape-preferred orientation of isotropic material is assumed. The elastic tensor of the effective anisotropic medium can be described by five independent elastic constants. The matrix of elastic constants for a horizontally transverse isotropic medium (HTI) is given by Ikelle and Amundsen (2005)

$$c_{ij} = \begin{pmatrix} c_{11} & c_{13} & c_{13} & 0 & 0 & 0 \\ c_{13} & c_{33} & c_{33} - 2c_{44} & 0 & 0 & 0 \\ c_{13} & c_{33} - 2c_{44} & c_{33} & 0 & 0 & 0 \\ 0 & 0 & 0 & c_{44} & 0 & 0 \\ 0 & 0 & 0 & 0 & c_{66} & 0 \\ 0 & 0 & 0 & 0 & 0 & c_{66} \end{pmatrix}.$$

The effective elastic constants of the HTI-medium are derived by an analytical solution (Ikelle and Amundsen 2005).

References

Backus GE (1962) Long-wave elastic anisotropy produced by horizontal layering. J Geophys Res 67:4427–4440

Bagley B, Nyblade AA (2013) Seismic anisotropy in eastern Africa, mantle flow, and the African superplume. Geophys Res Lett 40:1500–1501. doi:10.1002/grl.50315

Batte AG, Rümpker G, Lindenfeld M, Schumann A (2014) Structurally controlled seismic anisotropy above small earthquakes in crustal rocks beneath the Rwenzori region, Albertine Rift, Uganda. J Afr Earth Sci (submitted)

Ben Ismail W, Mainprice D (1998) An olivine fabric database: an overview of upper mantle fabrics and seismic anisotropy. Tectonophysics 296:145–158

Bendick R, McClusky S, Bilham R, Asfaw L, Klemperer S (2006) Distributed Nubia–Somalia relative motion and dike intrusion in the main Ethiopian rift. Geophys J Int 165:303–310

Bosworth W, Strecker MR, Bliniuk PM (1992) Integration of East African paleostress and present-day stress data: implications for continental stress field dynamics. J Geophys Res 97:11851–11865

Chorowicz J (2005) The East African Rift system. J Afr Earth Sci 43:379–410

Crampin S (1991) Wave propagation through fluid-filled inclusions of various shapes: interpretation of extensive-dilatancy anisotropy. Geophys J Int 104:611–623

Ebinger CJ (1989) Tectonic development and the western branch of the East African rift system. Geol Soc Am Bull 101:885–903

Foley SF (1992) Vein-plus-wall-rock melting mechanisms in the lithosphere and the origin of potassic alkaline magmas. Lithos 28:435–453

Foley SF, Link K, Tiberindwa JV, Barifaijo E (2012) Patterns and origin of igneous activity around the Tanzanian craton. J Afr Earth Sci 62:1–18

Fouch MJ, Rondenay S (2006) Continental seismic anisotropy. Phys Earth planet Int 158:292–320

Gao SS, Davis PM, Liu H, Slack PD, Rigor AW, Zorin YZ, Mordvinova VV, Kozhevnikov VM, Meyer RP (1994) Seismic anisotropy and mantle flow beneath the Baikal rift zone. Lett Nat 371:149–151

Gao SS, Davis PM, Liu H, Slack PD, Rigor AW, Zorin YZ, Mordvinova VV, Kozhevnikov VM, Logatchev NA (1997) SKS splitting beneath the continental rift zones. J Geophys Res 102:22781–22797

Gao SS, Liu KH, Abdelsalam MG (2010) Seismic anisotropy beneath the Afar depression and adjacent areas: implications for mantle flow. J Geophys Res 115. doi:10.1029/2009JB007141

Gummert M, Lindenfeld M, Wölbern I, Rümpker G, Kasereka CM, Batte AG (2014) Crustal structure and high-resolution Moho topography across the Rwenzori region (Albertine rift) from P-receiver functions. Submitted to Geological Society, London, Special Publications

Hammond JOS, Kendall JM, Angus D, Wookey J (2010) Interpreting spatial variations in anisotropy: insights into the main Ethiopian rift from SKS waveform modeling. Geophys J Int 181:1701–1712

Heintz M, Kennett BLN (2005) Continental scale shear-wave splitting analysis: investigation of seismic anisotropy underneath the Australian continent. Earth Planet Sci Lett 236:106–119

Holtzman BK, Kendall JM (2010) Organized melt, seismic anisotropy, and plate boundary lubrication. Geochem Geophys Geosyst 11:Q0AB06. doi:10.1029/2010GC003296

Ikelle LT, Amundsen L (2005) Introduction to petroleum seismology. Society of Exploration Geophysicists, Tulsa

Karato SI (2003) The dynamic structure of the deep Earth: an interdisciplinary approach. Princeton University Press, Princeton

Kendall JM (1994) Teleseismic arrivals at a mid-ocean ridge: effects of mantle melt and anisotropy. Geophys Res Lett 21:301–304

Kendall JM, Stuart GW, Ebinger CJ, Bastow ID, Keir D (2005) Magma assisted rifting in Ethiopia. Nature 433:146–148

Kumazawa M, Anderson OL (1969) Elastic moduli, pressure derivatives, and temperature derivatives of single-crystal olivine and single-crystal forsterite. J Geophys Res 74:5961–5972

Lindenfeld M, Rümpker G (2011) Detection of mantle earthquakes beneath the East African rift. Geophys J Int 186:1–5

Lindenfeld M, Rümpker G, Batte A, Schumann A (2012) Seismicity at the Rwenzori Mountains, East African rift: earthquake distribution, magnitudes and source mechanisms. Solid Earth 3:251–264

Link K, Koehn D, Barth MG, Tiberindwa JV, Barifaijo E, Aanyu K, Foley SF (2010) Continuous cratonic crust between the Congo and Tanzania blocks in western Uganda. Int J Earth Sci 99(7):1559–1573. doi:10.1007/s00531-010-0548-8 (Special Issue "Long-term Rift Evolution")

Long MD, Silver PG (2009) Shear wave splitting and mantle anisotropy: measurements, interpretations, and new directions. Surv Geophys 30:407–461

Nicolas A, Christensen NI (1987) Formation of anisotropy in upper mantle peridotites: a review, in composition, structure, and dynamics of the lithosphere–asthenosphere system. Geodyn Ser 16, Fuchs K and Froidevaux C (ed), AGU, Washington, DC, pp 111–123

Nicolas A, Achauer U, Daignieres M (1994) Rift initiation by lithospheric rupture. Earth Planet Sci Lett 123:281–298

Nyblade AA, Brazier RA (2002) Precambrian lithosphere controls on the development of the East African rift system. Geology 30:755–758

Rosenthal A, Foley SF, Pearson DG, Nowell GM, Tappe S (2009) Petrogenesis of strongly alkaline primitive volcanic rocks at the propagating tip of the western branch of the East African rift. Earth Planet Sci Lett 284:236–248

Rümpker G, Ryberg T (2000) New "Fresnel-zone" estimates for shear-wave splitting observations from finite-difference modeling. Geophys Res Lett 27:2005–2008

Rümpker G, Silver PG (1998) Apparent shear-wave splitting parameters in the presence of vertically varying anisotropy. Geophys J Int 135:790–800

Ryberg T, Rümpker G, Tittgemeyer M, Wenzel F (2002) Finite-difference simulations of seismic wavefields in isotropic and anisotropic Earth models. In: Krause E, Jäger W (eds) High performance computing in science and engineering 2001. Springer, Berlin, pp 35–47

Sander S, Rosendhal BR (1989) The geometry of rifting in Lake Tanganyika, East Africa. J Afr Earth Sci 8:323–354

Savage MK (1999) Seismic anisotropy and mantle deformation: what have we learned from shear wave splitting? Rev Geophys 37:65–106

Silver PG (1996) Seismic anisotropy beneath the continents: probing the depths of geology. Annu Rev Earth Planet Sci 24:385–432

Silver PG, Chan WW (1991) Shear-wave splitting and subcontinental mantle deformation. J Geophys Res 96:16429–16454

Stamps DS, Calais E, Saria E, Hartnady CH, Nocquet JM, Ebinger CJ, Fernandes RM (2008) A kinematic model for the East African rift. Geophys Res Lett 35:L05304. doi:10.1029/2007GL032781

Tommasi A (1998) Forward modeling of the development of seismic anisotropy in the upper mantle. Earth Planet Sci Lett 160:1–13

Vauchez A, Tommasi A, Barroul G, Mamus J (2000) Upper mantle deformation and seismic anisotropy in continental rifts. Phys Chem Earth A 25(2):111–117

Walker KT, Nyblade AA, Klemperer SL, Bokelmann GHR, Owens TJ (2004) On the relationship between extension and anisotropy: constraints from shear-wave splitting across the East African Plateau. J Geophys Res 109. doi:10.1029/2003JB002866

Wallner H, Schmeling H (2010) Rift induced delamination of mantle lithosphere and crustal uplift: a new mechanism for explaining Rwenzori Mountains extreme elevation? Int J Earth Sci doi:10.1007/s00531-010-0521-6

Wölbern I, Rümpker G, Link K, Sodoudi F (2012) Melt infiltration of the lower lithosphere beneath the Tanzania craton and the Albertine rift inferred from S receiver functions. Geochem Geophys Geosyst 13(1). doi:10.1029/2012GC004167

Wölbern I, Löbl U, Rümpker G (2014) Crustal origin of trench-parallel shear-wave fast polarizations in the Central Andes. Earth Planet Sci Lett 392:230–238. doi:10.1016/j.epsl.2014.02.032

Wolfe CJ, Silver PG (1998) Seismic anisotropy of oceanic upper mantle: shear-wave splitting methodologies and observations. J Geophys Res 103:749–771

Zhang S, Karato SI (1995) Lattice preferred orientation of olivine aggregates deformed in simple shear. Nature 375:774–777. doi:10.1038/375774a0